

Design of Belt-Tensioner Systems for Dynamic Stability

A. G. Ulsoy
Assistant Professor.

J. E. Whitesell
Assistant Professor.

M. D. Hooven*
Graduate Research Assistant.

Department of Mechanical Engineering
and Applied Mechanics
and Center for Robotics
and Integrated Manufacturing,
University of Michigan,
Ann Arbor, MI 48109

Belt drive systems are an effective means for power transmission which offer the advantages of light weight, low cost, quietness, and efficiency. Recently in automotive applications there has been a trend to power several accessories with a single drive belt in order to reduce overall vehicle size and weight. Since these belts are typically longer than conventional belts, a tensioner component is added to maintain acceptable belt tension levels. In this paper we describe several potential instability mechanisms for belt-tensioner systems, and present a design methodology to ensure good dynamic performance of such systems. A mathematical model of the belt-tensioner system, and numerical solution methods, are utilized to develop a computer-aided design procedure. Numerical results, and confirming experimental data, are presented for a particular automotive belt-tensioner system.

1 Introduction

The vibration of axially moving belts belongs to a class of problems referred to as axially moving material vibration problems [1]. This class includes such diverse technologies as band saws [2]; moving threadlines [3]; power transmission chains [4]; pipes transporting fluids [5]; and moving belts [6, 7, 8, 9, 10]. In addition to resonance due to direct excitation, axially moving materials can exhibit a standing wave (or divergence buckling) type instability at a critical speed [11], a dynamic (or flutter) type instability at speeds above the critical [12], and Mathieu type instabilities due to parametric excitation [9, 11, 13]. Reviews of this diverse literature can be found in [1, 2].

The purpose of this paper is to model and analyze the transverse vibration and stability of coupled belt-tensioner systems, to develop a computer-aided design methodology, and to provide general recommendations for design. As shown in Fig. 1, the tensioner pulley is placed between spans 1 and 2 and is pinned to a tensioner arm of length l_t . The tensioner arm is attached to a torsional spring, with spring constant K_t , at the pivot point P_3 . This paper will show that the tensioner plays several important roles affecting the dynamic performance of the belt system. These include maintaining an acceptable static belt tension, reducing belt tension variations due to dynamic loading, and increasing the critical belt speed by introducing pulley compliance. The engineering problem of interest is an automotive accessory drive system, although similar problems may be encountered in other technological areas.

In the belt-tensioner system the belt can exhibit some

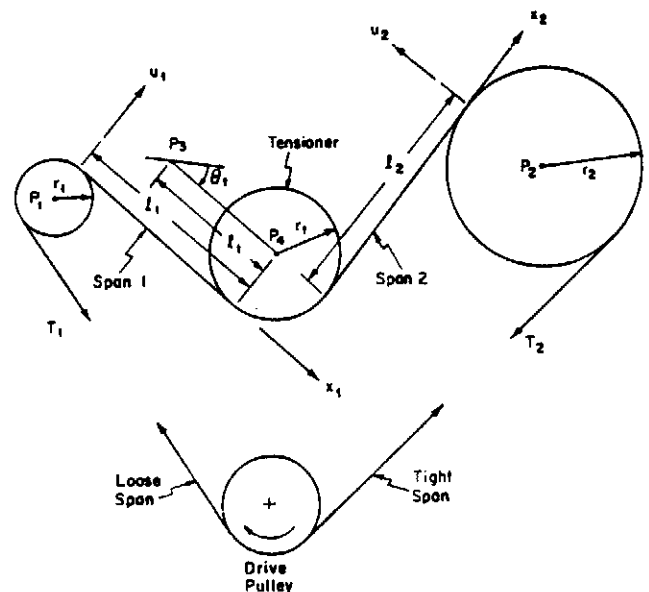


Fig. 1 Schematic of a belt-tensioner system

combination of longitudinal, torsional, and transverse vibration. Since the natural frequencies associated with longitudinal and torsional vibrations are quite high for typical belt material and geometries, only transverse belt vibrations are considered here. There are four primary transverse instability mechanisms that must be considered in the design of belt-tensioner systems; these are schematically illustrated in Fig. 2 and described below:

1 Tensioner resonance occurs when an excitation frequency (e.g., due to accessory loading) is equal to the natural frequency of the tensioner.

2 Belt resonance can also occur if a transverse excitation frequency is equal to a belt natural frequency.

*Presently Project Engineer, Cordis Corporation.

Contributed by the Technical Committee on Vibration and Sound for presentation at the Design Engineering Technical Conference, Cincinnati, Ohio, September 10-13, 1985 of THE AMERICAN SOCIETY OF MECHANICAL ENGINEERS. Manuscript received at ASME Headquarters, May 13, 1985. Paper No. 85-DET-6.

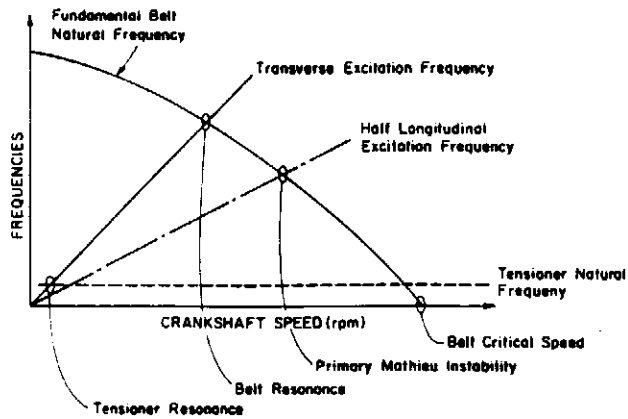


Fig. 2 Four mechanisms of transverse instability in belt-tensioner systems

3 A Mathieu type instability, due to parametric excitation, can also occur when $n^2/2$ times the belt tension variation frequency is approximately equal to a belt natural frequency, particularly the fundamental ($n = 1, 2, 3 \dots$). This mechanism has been described in detail in [14], and in [11] for moving belts.

4 A standing wave instability occurs when the belt fundamental natural frequency goes to zero at a belt critical speed equal to the wave velocity of the material [11].

In the automotive accessory drive system of interest the belt resonance mechanism was not active, since the belt excitation is longitudinal rather than transverse. The longitudinal belt excitation is translated by the tensioner to transverse excitation, but the tensioner acts as a low pass filter and attenuates the higher frequencies which could otherwise lead to belt resonance problems. It was also found that tensioner resonance could be limited to engine speeds well below the operating speed range, and the belt critical speeds could be kept well above the operating speed range. Thus, the most important instability mechanism is the Mathieu type, and must be given careful consideration in the design of belt-tensioner systems.

In Section 2 we present a mathematical model of the coupled belt-tensioner vibration problem, and also a numerical solution method based on finite differencing. For the purpose of model validation, experimental studies were also undertaken and are described in Section 3. Results from both the experiments and the analyses are presented and discussed in Section 4. Finally we summarize the results of these studies and present design recommendations in section 5.

2 Theory and Analysis

The tensioner, shown in Fig. 3, is modeled as a single degree of freedom system which is subject to an input moment due to

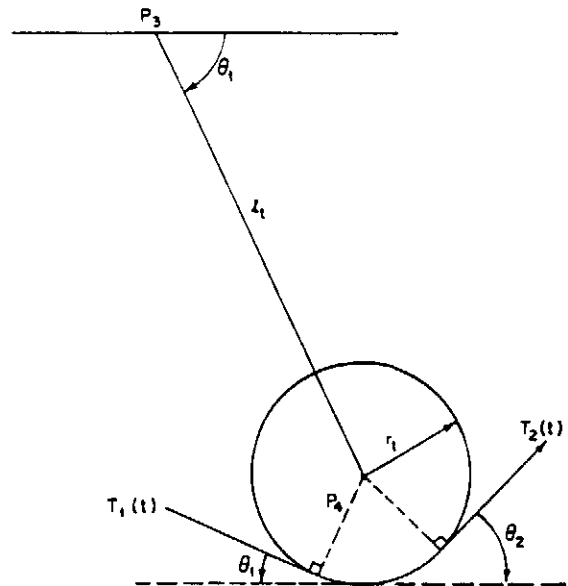


Fig. 3 Schematic of the tensioner

the belt tension. The moment of inertia of the tensioner pulley about its center (P_4 in Fig. 3) is neglected, and the instantaneous belt tension in each span is assumed to be equal (i.e., $T_1 = T_2$ in Fig. 3). The equation of motion is obtained by a dynamic equilibrium of moments about the pivot point P_3 in Fig. 3 (see Appendix A for the complete derivation),

$$I_t \ddot{\theta}_i + C_t \dot{\theta}_i + K_t \theta_i = K_t \theta_0 + P_t + f(\theta_i) \quad (1)$$

where θ_i is the tensioner arm angle, I_t is the effective moment of inertia about P_3 , C_t is the effective viscous damping coefficient, K_t is the torsional spring stiffness, θ_0 is the initial tensioner arm angle, P_t is the tensioner preload moment, and $f(\theta_i)$ is a nonlinear moment due to the belt tension.

The equations of motion for the transverse vibration of the belt are based on an axially moving string model [11]. The bending stiffness of the belt is neglected, since the belt tension is assumed to dominate the transverse stiffness. It is further assumed that the belt axial velocity c is constant, and that the transverse displacement of the belt from equilibrium $u(x, t)$ is small. The equation of motion for each span is

$$\rho A u_{,tt} + 2\rho A c u_{,xt} + (\kappa \rho A c^2 - T) u_{,xx} + \beta(u_{,t} + c u_{,x}) = 0 \quad (2)$$

where ρA is the mass per unit length of the belt, $u(x, t)$ is the belt displacement from equilibrium, T is the belt tension, κ is the pulley support system constant, and β is the belt damping coefficient. Equation (2) is used for each belt span with simple support boundary conditions at $x_1 = 0$ and $x_2 = l_2$. At $x_1 = l_1$ and $x_2 = 0$ the belt is subject to a time varying transverse tensioner force. Thus, the tensioner is excited by the belt

Nomenclature

A = belt cross-sectional area	about pivot point P_3 (see Figs. 1 and 3)	γ = nondimensional belt tension variation amplitude
c = belt axial velocity	r_i = radius of pulley i ($i = 1, 2$)	θ_0 = initial static tensioner arm angle
c^* = nondimensional belt velocity = $c / (T_0 / \kappa \rho A)^{1/2}$	r_t = radius of tensioner pulley	$\theta_i(t)$ = tensioner arm angle
C_t = tensioner viscous damping coefficient	t = time	κ = pulley support constant: $0 \leq \kappa \leq 1$ (and $\eta = 1 - \kappa$)
I_t = tensioner effective moment of inertia about pivot point P_3 (see Figs. 1 and 3)	T_i = belt tension in span i ($i = 1, 2$)	ρ = belt material mass density
K_t = tensioner spring constant	T_0 = initial static belt tension	ω_e = one-half the belt tension variation frequency
l_i = length of span i ($i = 1, 2$)	$u(x, t)$ = belt transverse displacement	ω_n = belt natural frequency for mode n
l_t = length of tensioner arm	x = spatial coordinate along belt longitudinal axis	
P_t = tensioner preload moment	β = belt viscous damping coefficient	

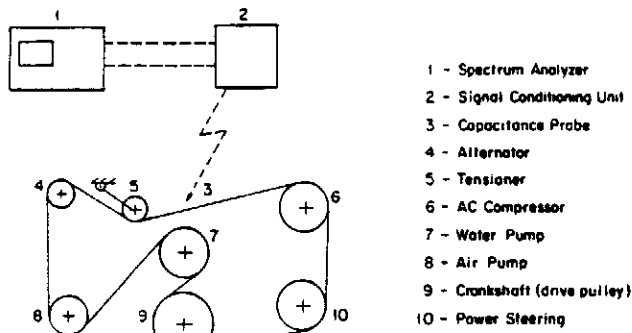


Fig. 4 Schematic of the experimental setup

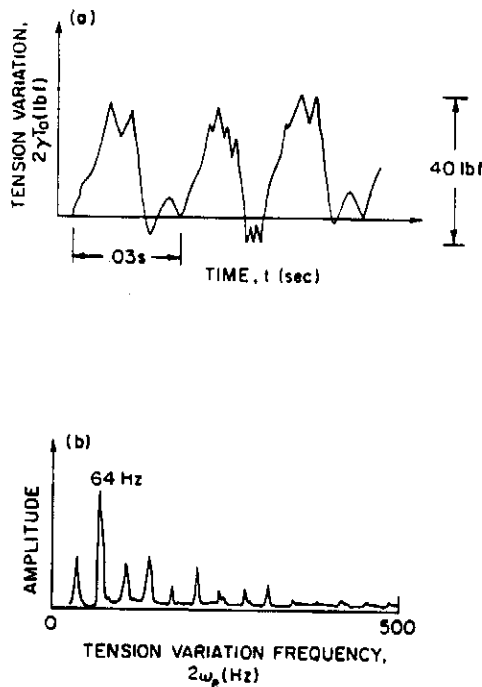


Fig. 5 Typical compressor characteristics at 1500 rpm: (a) tension variation versus time; (b) spectrum

tension in equation (1), and the tensioner motion excites the belt through boundary conditions at $x_1 = l_1$ and $x_2 = 0$. Note that the contact points between the belt and the pulleys, and the span lengths l_1 and l_2 , depend on the tensioner motion and the system geometry (see Fig. 1). The necessary relationships are derived in Appendix B.

The belt is subject to parametric excitation due to variations in the tension T in equation (2). These belt tension variations arise from the loading of the pulleys by the belt-driven accessories (e.g., air conditioning compressor) in the automotive system of interest. They may also arise in other systems due to pulley eccentricities. Thus, the belt tension is represented by [11]

$$T(t) = T_0(1 + (\eta\rho Ac^2/T_0) + 2\gamma \cos 2\omega_p t) \quad (3)$$

where T_0 is the initial static belt tension, and $2\gamma \cos 2\omega_p t$ is used to represent the tension variation produced by the belt-driven accessories. The pulley support constant, $0 \leq \eta \leq 1$, represents the compliance of the pulley support system, and $\kappa = 1 - \eta$ in equation (2). The effect of κ or η on the belt vibration problem has been thoroughly described in [11], and a brief discussion is included in Appendix C.

The equations (1)–(3), together with boundary conditions at $x_1 = 0, x_1 = l_1, x_2 = 0$, and $x_2 = l_2$, and initial conditions for θ , and $u(x, t)$ in each span describe the vibration and

stability of the coupled belt-tensioner system. The boundary conditions at $x_1 = 0$ and $x_2 = l_2$ are given by $u = 0$. The boundary conditions at $x_1 = l_1$ and $x_2 = 0$ are $u = U(\theta, t)$. The transverse boundary displacements $U(\theta, t)$ for each span are calculated from the geometry and tensioner motion as described in Appendix B.

The numerical solution of the coupled belt-tensioner system can be obtained utilizing a finite difference method in both the spatial and temporal variables. Forward differencing in time is used for both the tensioner and belt equations. A hybrid differencing scheme is used to spatially discretize the belt equations in each span, i.e.,

$$\frac{\partial u_j}{\partial x} = \frac{m(1-c^*)}{2} u_{i+1,j} + mc^* u_{i,j} - \frac{m(1+c^*)}{2} u_{i-1,j} \quad (4)$$

This is a weighted combination of central and backward differencing, where m is the number of spatial segments, $c^* = c/(T_0/\kappa\rho A)^{1/2}$ is the nondimensional belt speed, and the indices i and j refer to the spatial and temporal segments, respectively. This hybrid scheme results in a central difference at low ($c^* \ll 1$) belt speeds, and a backward difference at high ($c^* \approx 1$) belt speeds. The numerical solution algorithm proceeds as follows:

- (i) Initialize tensioner and belt variables and set $j = 0$.
- (ii) Solve for θ , at time $t = j\Delta t$, and compute the transverse displacements at the belt-tensioner contact points.
- (iii) Solve for the belt transverse displacements $u_{i,j}$ for $i = 1, 2, \dots, m-1$ for both spans given the boundary conditions $u_{0,j}$ and $u_{m,j}$ computed in (ii).
- (iv) Set $j = j + 1$ and go to (ii) if $(j + 1)\Delta t \leq t_{max}$, otherwise stop.

3 Experimental Studies

To validate the mathematical model described in the previous section an automotive accessory belt-drive system was tested in a dynamometer test cell at the Walter Lay Automotive Laboratory, a facility of the Department of Mechanical Engineering and Applied Mechanics at the University of Michigan. A production automotive engine, complete with belt-driven accessories, was motored by the dynamometer throughout the normal operating speed range. The belt vibration was monitored using a capacitance type proximity probe, the tensioner vibration was measured using a reluctance type proximity probe, and the loading from the air conditioning compressor was measured by attaching strain gages to the compressor pulley. The experimental setup is schematically illustrated in Fig. 4, where only the capacitance probe is shown for clarity.

Tests were run with two different air conditioning (AC) compressor units, and the following data were collected:

- (i) belt natural frequency spectra at selected crankshaft rotational speeds between 1000 and 4500 rpm with no AC compressor loading;
- (ii) compressor torque amplitude versus time data and frequency spectra for the two AC compressors at selected crankshaft speeds;
- (iii) belt and tensioner frequency spectra at selected crankshaft rotational speeds with AC compressor loading.

The data from (i) were used to calculate a value of the pulley support constant κ . As described in [11] the value of κ determines the rate at which the belt natural frequencies decrease with increasing belt speed. A value of $\kappa = 0.3$ was obtained for the experimental system with both compressors. The data in (ii) were used to characterize the excitation from

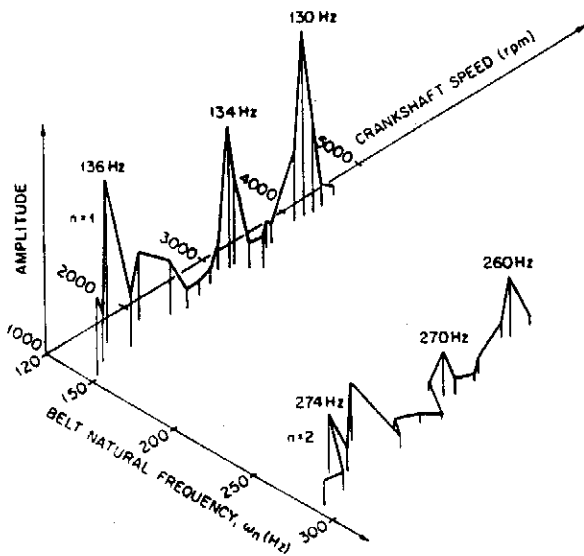


Fig. 6 Experimental results for the two lowest belt natural frequencies versus crankshaft speed

the AC compressors. Figure 5 shows a typical time history and spectrum for one of the AC compressors tested. This type of excitation data was used to determine the values for the tension variation amplitude ($2\gamma T_0$) and frequency ($2\omega_e$) in equation (3). It should be noted that, although the excitation waveform is more complex, it is represented by a single cosine function in (3). The data in (iii) above was used to determine the crankshaft rotational speeds at which tensioner resonance and belt Mathieu instabilities occur. This data is presented in the next section and compared to the results obtained from the analyses.

4 Results and Discussion

The experimental results which identify the Mathieu instability regions are shown in Fig. 6. This is an isometric plot which shows the change in the amplitudes of the power spectra of the first and second vibration modes as a function of crankshaft rotational speed. While actual values of the amplitudes are not very meaningful, large amplitude regions do indicate the speed ranges where Mathieu instabilities occur. Prolonged operation of the engine and AC compressor at one of these speeds (e.g., with "cruise control" on a flat highway) would probably result in belt failure.

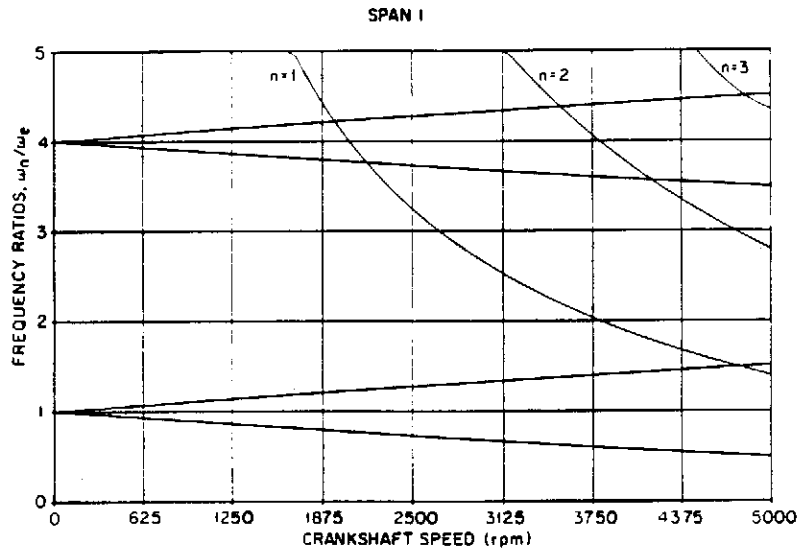


Fig. 7 Frequency ratios (ω_n/ω_e) versus crankshaft speed for Span 1 based on an uncoupled analysis

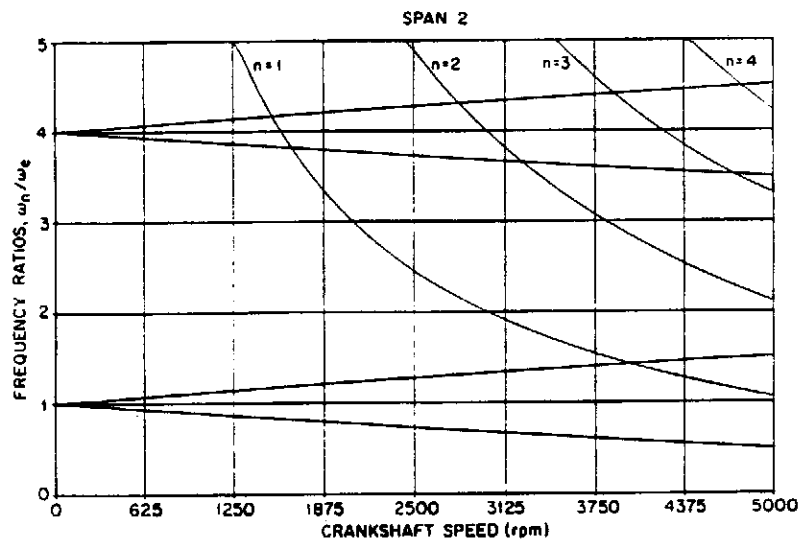


Fig. 8 Frequency ratios (ω_n/ω_e) versus crankshaft speed for Span 2 based on an uncoupled analysis

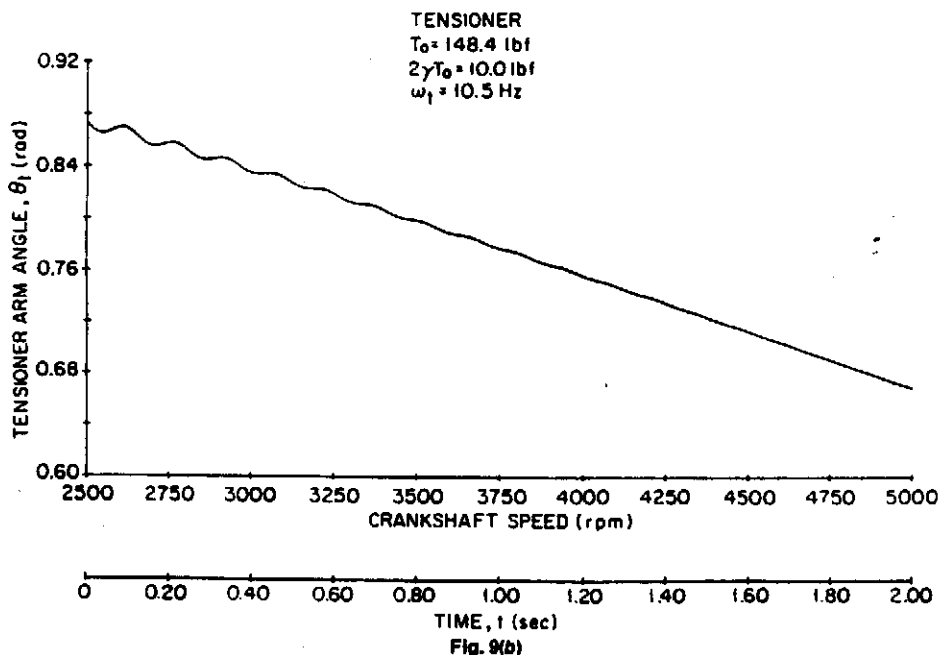
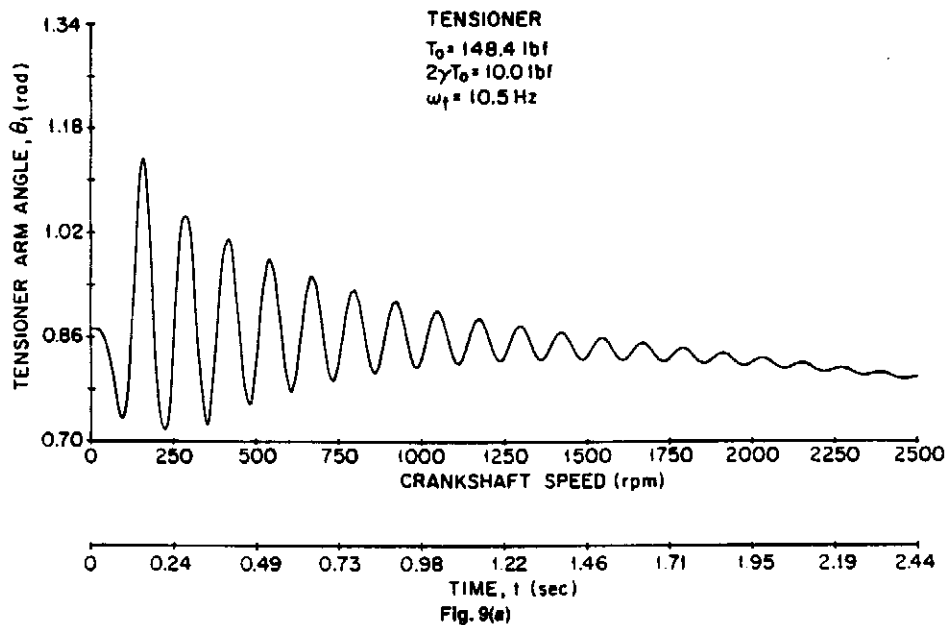


Fig. 9 Tensioner arm angle versus time based on a coupled analysis: (a) 0 to 2500 rpm sweep; (b) 2500 to 5000 rpm sweep

Two sets of analytical results were also generated for this automotive system for comparison to the experimental data. The results shown in Figs. 7 and 8 are based on an uncoupled analysis of the two belt spans as described in [11]. The curves in the figures labeled $n = 1, 2,$ and 3 show the values of (ω_n/ω_e) , while the lines emanating from the points $(\omega_n/\omega_e) = 1$ and 4 represent the Mathieu instability criteria as a function of the belt velocity c [11]. The intersections of these curves and lines indicate *potential* Mathieu instability regions about the intersection points. These potential instability regions may be "narrow" or even "closed" depending on the amplitude of the belt tension variation and on the belt damping [11, 14]. This uncoupled analysis does not account for these factors. Note also that at low crankshaft rotation speeds (i.e., $c \approx 0$) we have the usual Mathieu instability criteria $(\omega_n/\omega_e) = i^2$ where $i = 1, 2, 3, \dots$, etc. This is the approximate criterion indicated in Fig. 2 for $n = 1$ and $i = 1$.

Figures 9-11 show the results from a simulation of this automotive system based on the coupled belt-tensioner

analysis in Section 2. These figures show the vibration of the tensioner and the midpoint of the belt in each adjacent span as a function of time. The crankshaft rotational speed is swept through a specified range during the simulation, and crankshaft rotational speeds are also given along the horizontal axis. The modeling of the belt vibration was based on a constant belt speed, thus the rotational speed range must be swept in a quasi-steady manner (i.e., the change in the rotational speed at each time step must be small). These results are presented in two parts, for a 0 to 2500 rpm and 2500 to 5000 rpm range of the crankshaft rotational speed. The tensioner resonance occurs at a low speed (< 250 rpm), and the amplitude of the tensioner motion is quite small for speeds > 2000 rpm. The tensioner equilibrium position shifts upward (i.e., θ_t decreases) with increasing speed due to belt tension increase as shown in equation (3). The belt vibration in both spans is due to the tensioner motion at low speeds. At higher speeds we observe large amplitude vibrations at certain operating speed ranges which arise from the belt tension

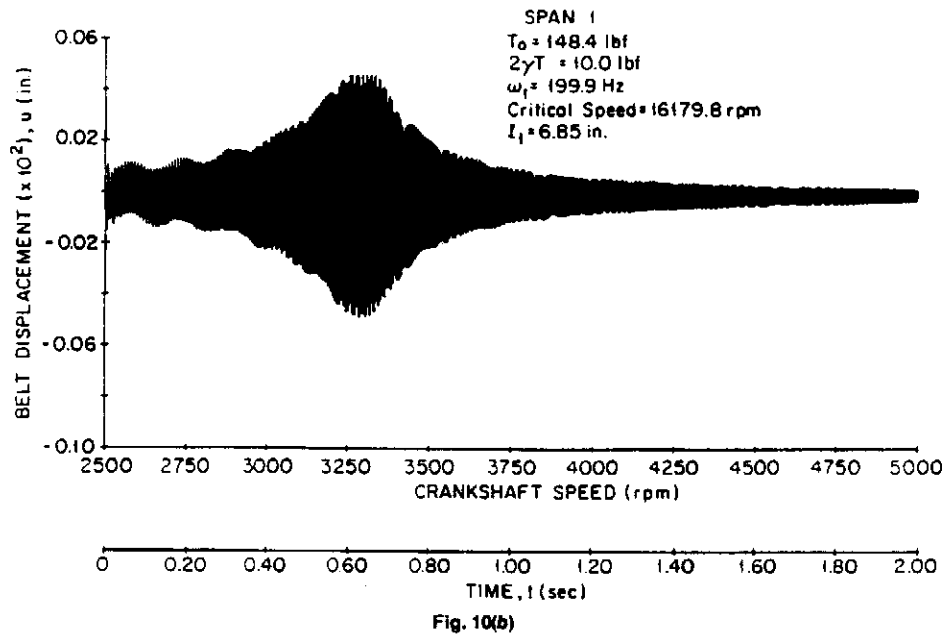
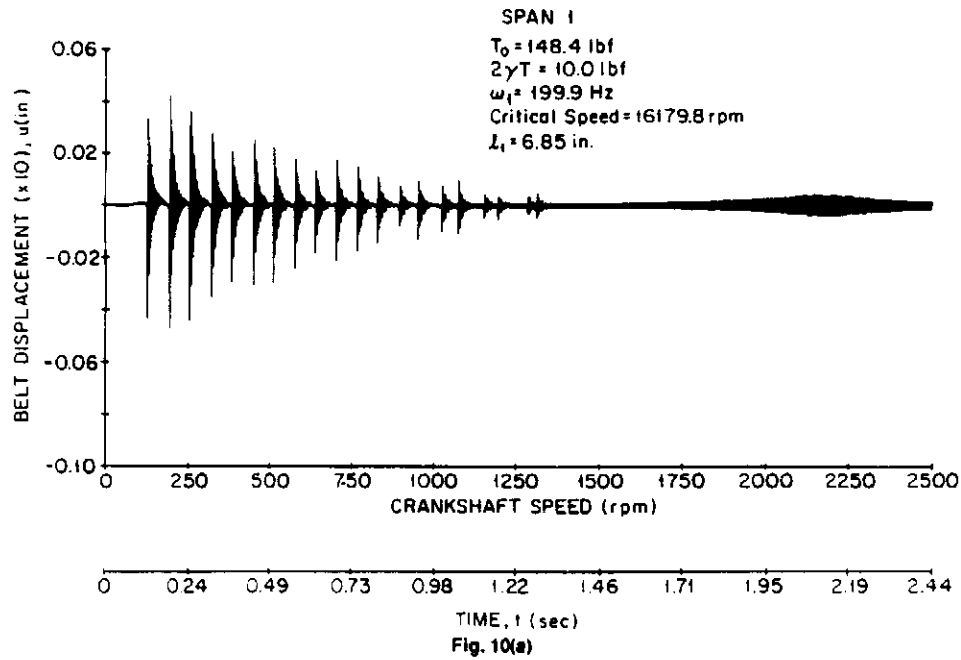


Fig. 10 Belt midpoint displacement in Span 1 versus time based on a coupled analysis: (a) 0 to 2500 rpm sweep; (b) 2500 to 5000 rpm sweep

variations. These "bulges" in the envelope of the belt vibration indicate operating speed ranges where Mathieu instabilities are expected to occur.

The results indicating operating speeds at which Mathieu instabilities are expected to occur (from Figs. 6 to 11) are compared in Table 1. Although the results from the uncoupled analysis are useful there are certain instability regions predicted which were not experimentally observed, probably since the effect of damping is to make some of these regions closed for small tension variation amplitudes [11, 14]. The results from the coupled analysis are even more encouraging. The crankshaft speed predictions from the coupled analysis are within 5–15 percent of those experimentally observed. This is considered to be reasonable, especially since it is difficult to pinpoint these speeds experimentally due to the violent belt dynamic behavior. The model also characterizes the tension variation as a single cosine function, whereas the

actual wave form is more complex (see Fig. 5). The uncoupled analysis is computationally much more efficient than the coupled analysis, and gives useful results. Thus, it should be preferred for preliminary design work. The coupled analysis gives a more complete picture of the dynamic behavior of the belt-tensioner system since the amplitude of belt tension variation and belt damping can be directly accounted for. The results of the coupled analysis may also be easier to interpret for the designer, since he or she can directly observe large amplitude vibration regions (bulges) as in Figs. 10 and 11. The two analytical methods complement each other well as design tools.

5 Summary and Conclusions

A mathematical model and numerical solution method for analyzing the transverse vibration and stability of belt-

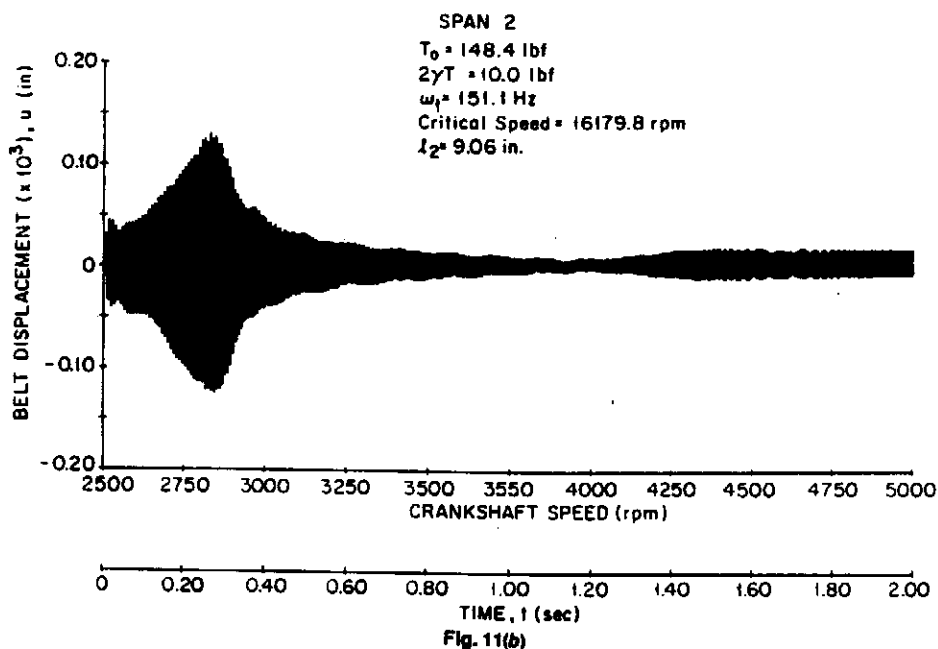
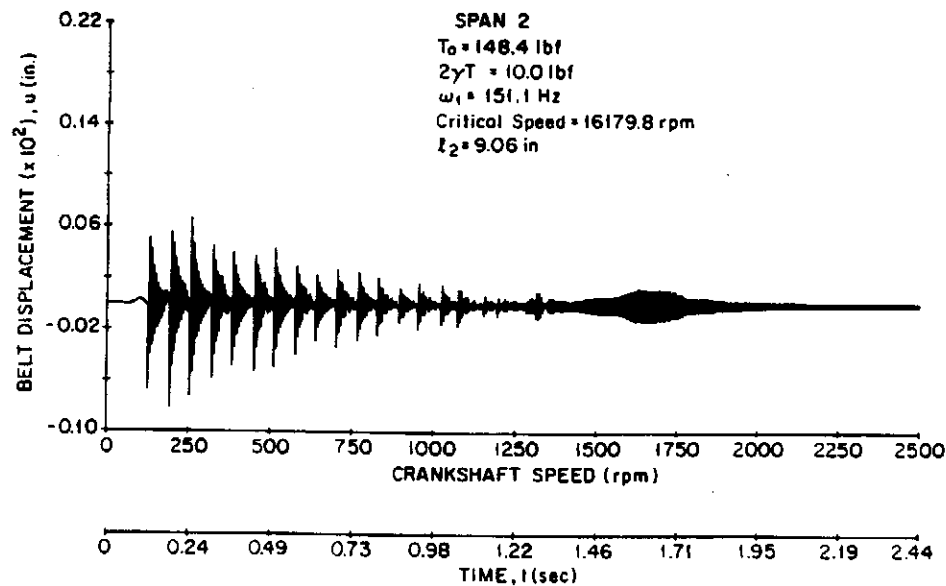


Fig. 11 Belt midpoint displacement in Span 2 versus time based on a coupled analysis: (a) 0 to 2500 rpm sweep; (b) 2500 to 5000 rpm sweep

tensioner systems has been presented. The model has been validated by comparison to experimental data collected on a production automotive accessory belt drive system.

There are four primary mechanisms for transverse belt instability: (i) tensioner resonance, (ii) belt resonance, (iii) Mathieu instabilities due to belt tension variations, and (iv) belt critical speed. Tensioner resonance can be avoided by selecting a low tensioner spring constant such that excitation frequencies which could lead to tensioner resonance are kept below the operating speed range. If the excitation sources are primarily longitudinal, this will eliminate the belt resonance problem since the tensioner will act to attenuate high-frequency excitation which could otherwise excite belt natural frequencies. A low tensioner spring constant also acts to increase belt critical speed by introducing pulley compliance into the system. A final advantage of a soft tensioner spring is that it acts as a spring in series with the belt stiffness and reduces the magnitude of belt tension variations due to accessory loading. This helps to minimize the effects of the Mathieu instabilities.

The mathematical model and numerical solution method presented form the basis for a computer-aided design procedure for belt-tensioner systems. The effects of changes in geometric and operating parameters on the belt dynamic performance can be quickly and inexpensively evaluated. The uncoupled analysis for the belt and tensioner is computationally more efficient than the coupled belt-tensioner model and can be useful for preliminary design work.

Acknowledgments

The authors are pleased to acknowledge the financial support of the Ford Motor Company; the assistance of Mr. Dick Cronin, Mr. Reuben Slone, and Mr. Bob Messenger with testing and programming; the interest and support of the Dayco Belt Company; the technical support of the Walter E. Lay Automotive Laboratory staff; and the typing of the manuscript by Ms. Laura Hagerman.

Table 1 Comparison of measured and predicted values of crankshaft rotation speeds around which Mathieu instability regions are expected (Span 2)

Results from:	Crankshaft rotation speed (rpm)
	1575
Experiments* (Fig. 6)	2000 3100 4075
Uncoupled analysis (Figs. 7-8)	1500 (mode 1) 1600 (mode 1) 2800 (mode 2) 3200 (mode 2) 3900 (mode 3) 4000 (mode 1) 4700 (mode 3) 4800 (mode 4)
Coupled analysis (Figs. 9-11)	1500 1700 2900 4300 4800

*Tests run from 1000 to 4500 rpm only.

References

- 1 Mote, C. D., Jr., "Dynamic Stability of Axially Moving Materials," *Shock and Vibration Digest*, Vol. 4, No. 4, Apr. 1972, pp. 2-11.
- 2 Ulsoy, A. G., Mote, C. D., Jr., and Szymani, R., "Principal Developments in Band Saw Vibration and Stability Research," *Holz als Roh- und Werkstoff*, Vol. 36, July 1978, pp. 273-280.
- 3 Swope, R. D., and Ames, W. R., "Vibrations of a Moving Threadline," *Journal of Franklin Institute*, Vol. 275, No. 1, 1963, pp. 36-55.
- 4 Mahalingam, S., "Transverse Vibrations of Power Transmission Chains," *British Journal of Applied Physics*, Vol. 8, 1957, pp. 145-148.
- 5 Housner, G. W., "Bending Vibrations of a Pipeline Containing Flowing Fluid," *ASME Journal of Applied Mechanics*, Vol. 19, 1952, pp. 205-209.
- 6 Chubachi, T., "Lateral Vibration of Axially Moving Wire or Belt Form Materials—Experiment," *Bulletin of the Japanese Society of Mechanical Engineers*, Vol. 23, No. 127, 1957, pp. 205-210.
- 7 Chubachi, T., "Lateral Vibration of Axially Moving Wire or Belt Form Materials," *Bulletin of the Japanese Society of Mechanical Engineers*, Vol. 1, No. 1, 1958, pp. 24-29.
- 8 Doyle, E., and Hornung, K. G., "Lateral Vibration of V-Belts," *ASME Paper No. 69-Vibr-29*, 1969.
- 9 Rhodes, J. E., Jr., "Parametric Self-Excitation of a Belt Into Transverse Vibration," *ASME Journal of Applied Mechanics*, Vol. 37, No. 4, 1970, pp. 1055-1060.
- 10 Lai, J., and Chen, C. H., "Vibration and Dynamic Stability of an Axially Moving Belt," *ASME Paper No. 71-Vibr-31*, 1971.
- 11 Mote, C. D., Jr., "A Study of Bandsaw Vibrations," *Journal of the Franklin Institute*, Vol. 279, No. 6, 1965, pp. 430-444.
- 12 Ulsoy, A. G., and Mote, C. D., Jr., "Vibration of Wide Band Saw Blades," *ASME Journal of Engineering for Industry*, Vol. 104, No. 1, Feb. 1982, pp. 71-78.
- 13 Mote, C. D., Jr., "Dynamic Stability of an Axially Moving Band," *Journal of the Franklin Institute*, Vol. 285, No. 5, pp. 239-346.
- 14 McLachlan, N. W., *Theory and Application of Mathieu Functions*, Oxford University Press, London, 1947.
- 15 Goyal, A. K., and Bentley, A. J., "New Criteria for Air Conditioning Belt Drive Design," *SAE Paper No. 710546*, June 1971.

APPENDIX A

Derivation of the Tensioner Equation of Motion

Referring to Fig. 3 and summing moments about the fixed pivot point P_3 , we equate the inertial moment to the sum of the moments caused by the torsional spring, the belt tension, gravity, and damping.

$$I_t \ddot{\theta}_1 = M_s + M_b + M_g + M_d \quad (A1)$$

where the tensioner moment of inertia is

$$I_t = m_{eff} l_t^2 \quad (A2)$$

and m_{eff} is the effective mass of the tensioner arm and pulley. The moment due to the torsional spring is

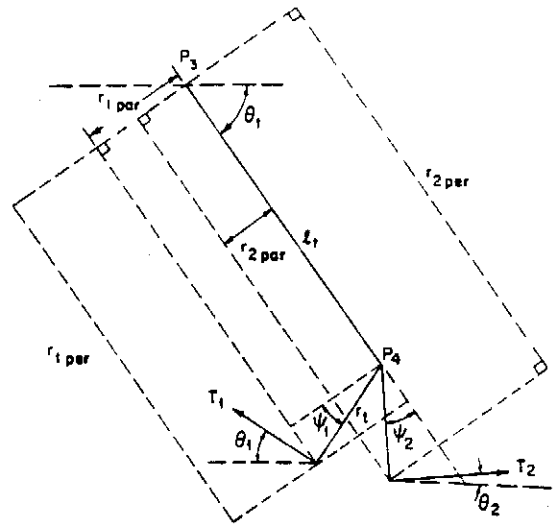


Fig. 12 Tensioner arm geometry for calculation of the moment due to belt tension

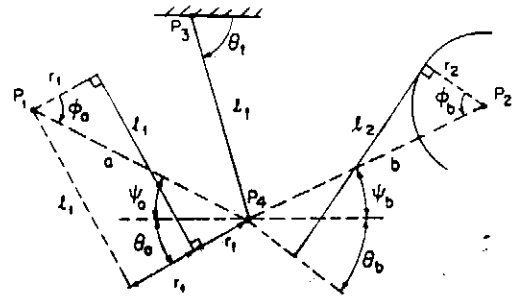


Fig. 13 Geometry for calculation of the span length dependence on tensioner arm angle, and the belt-tensioner contact points

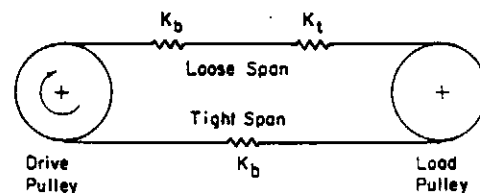


Fig. 14 Simplified schematic of the belt-tensioner system

$$M_s = K_t (\theta_0 - \theta_1) + P_t \quad (A3)$$

where K_t is the torsional spring constant, θ_0 is the initial tensioner arm angle, and P_t is the constant spring preload torque.

The calculation of the moment due to the belt tension about the fixed pivot point P_3 is performed in terms of components of the belt tension parallel and perpendicular to the tensioner arm. Referring to Figs. 3 and 12 we write

$$M_b = F_{1per} r_{1per} + F_{1par} r_{1par} + F_{2per} r_{2per} + F_{2par} r_{2par} \quad (A4)$$

where

$$\begin{aligned} r_{1per} &= l_t + r_1 \sin \psi_1 \\ r_{1par} &= r_1 \cos \psi_1 \\ r_{2per} &= r_1 \cos \psi_2 + l_t \\ r_{2par} &= r_1 \sin \psi_2 \\ F_{1per} &= T_1 \sin \psi_1 \\ F_{1par} &= T_1 \cos \psi_1 \end{aligned} \quad (A5)$$

